

# Effect of Nerve Variations on the Stimulus Current Level in a Wearable Neuromodulator for Migraine: A Modeling Study

Enver Salkim, *IEEE Student Member*, Arsam N. Shiraz, *IEEE Member* and  
Andreas Demosthenous, *IEEE Senior Member*

**Abstract**— Migraine is a socioeconomic burden, whose pharmaceutical and invasive treatment methods may have troublesome side-effects. A wearable neuromodulator targeting frontal nerve branches of trigeminal nerve may provide an effective solution to suppress or treat migraine. Such solutions have had limited efficacies. In this paper, using computational models, the relationship of this lack of efficacy to some neural variations is investigated. The results indicate that due to neuro-anatomic variations, different current levels may be required to achieve a sufficient level of neural stimulation. Thus, an optimized design should consider such variations across the patient group.

## I. INTRODUCTION

Migraine is the third most common neurological disorder and the seventh cause of disability. It may be diagnosed by several perceptions such as headache, nausea, vomiting, photophobia and phonophobia [1], [2]. The common complaint of migraine sufferers is generally the symptoms of pain originating in the frontal region of the head [3]. This may be due to the fact that migraine is primarily related to frontal nerve branches of the ophthalmic nerve [4]. Thus, a solution targeting this nerve directly may be of interest.

Available pharmaceutical treatments of migraine are not completely effective and have troublesome side-effects such as chronification [5]. Thus, there is a need for alternative treatments such as neuromodulation. Neuromodulation may be delivered invasively; however, this exposes the patients to the associated risks. Transcutaneous electrical nerve stimulation (TENS) is a non-invasive technique that is widely used to relieve pain [6]. In this technique, current is applied through the skin via surface electrodes to depolarize the neural tissue underneath. This has fewer complications compared with invasive methods. A solution based on transcutaneous supraorbital nerve stimulation for the prevention of episodic migraine is commercially available (Cefaly, CEFALY Technology, Liège, Belgium). By targeting sensory fibers in frontal nerves, namely supraorbital (SON) and supratrochlear (STN), migraine is alleviated [7]. This has been tested in double blind

This research was funded by PhD scholarship to E. Salkim by the Turkish Government, Ministry of National Education, Mus Alpaslan University.

E. Salkim, A. N. Shiraz and A. Demosthenous are with the Electronic and Electrical Department, University College London, Torrington Place, WC1E 7JE, London, UK.

{e-mail: enver.salkim.14; a.shiraz ; a.demosthenous@ucl.ac.uk}

randomized controlled trials [8] and post marketing survey studies [9], and has not been effective in many cases. This may be associated with the neuroanatomical variations across different subjects. No study has investigated this possible underlying cause of lack of efficacy in all subjects. This is partly due to the physical limitations of studying the neuroanatomy of individuals. However, using computational models of the human head, neural tissue and a neuromodulator, the effect of neuroanatomical variations may be readily investigated.

In this paper, a realistic three dimensional (3D) volume conductor model of the human head, the Cefaly's bipolar electrode configuration and a model of mammalian nerve fiber were developed. For various nerve variations based on existing anatomical data, the current level required to excite a population in the target nerve was modeled. Based on the results, conclusions may be drawn as to how such variations may affect the efficacy of the solution.

The paper is organized as follows. In Section II methods to generate the hybrid model (i.e., volume conductor and nerve model) and the subsequent investigations are described. The results and discussions are reported in Sections III and IV, respectively. Conclusions and future directions are discussed in Section V.

## II. METHODS

### A. MRI Data and Segmentation

To generate a realistic head model, a magnetic resonance image (MRI) dataset of a human head with  $0.5 \mu\text{m}$  isotropic resolution was acquired [10]. The dataset was composed of 350 slices, each of which comprised of  $480 \times 480$  pixels. Voxel dimensions were  $0.5 \times 0.5 \times 0.5 \text{ mm}$  for each of the  $x$ ,  $y$  and  $z$  planes. The raw image data slices were smoothed and the main tissue layers were identified as a new gray scale value in MATLAB v.R2015b (MathWorks, Inc., Natic M, USA). Smoothing is necessary to remove extra structural details around the target tissue layers to decrease computational time in the mesh generation process. The redefined dataset was imported to Simpleware ScanIP (Synopsys, Mountain View, USA) for image processing and data segmentation. The segmentation is a process in which the tissue layers are identified based on the grayscale data.

The physical extent of the MRI data was reduced from the lower boundary of the  $y$  plane and the upper boundary of the  $x$  plane until the minimum head volume was obtained by ensuring that the model was large enough for any electrical potential to decay sufficiently at the boundaries of the head segment. This is particularly beneficial in decreasing the

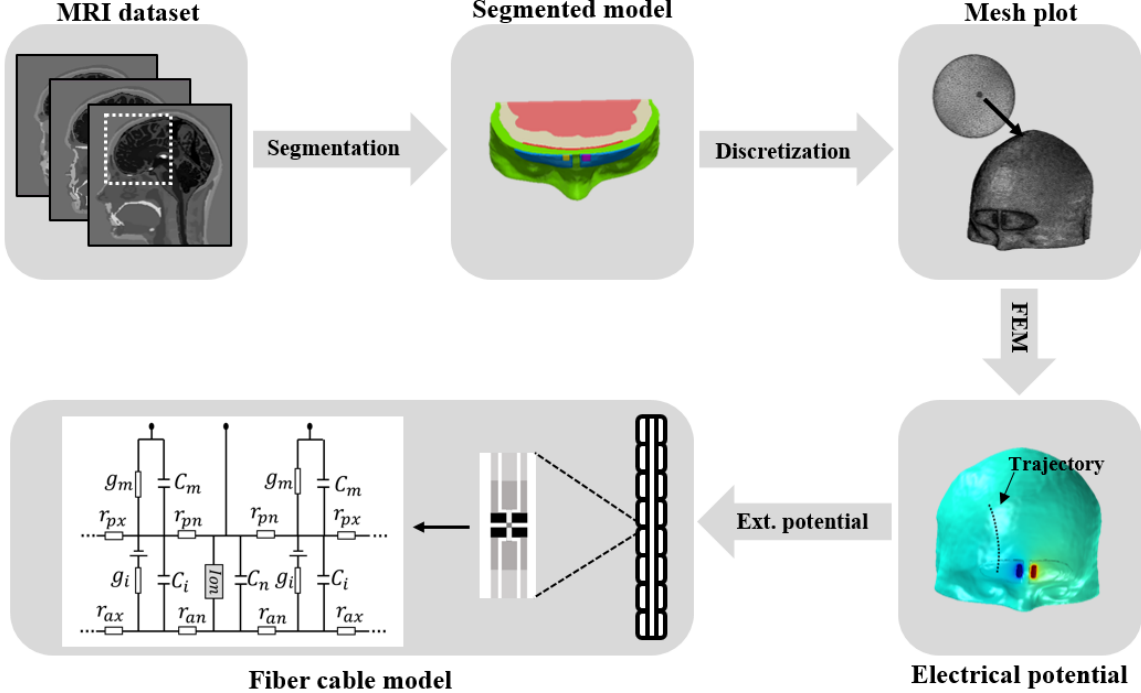


Figure 1. Showing the workflow of the modeling process. Starting from the MRI dataset a section of data shown by dotted square is segmented and a 3D model is developed. This model is then discretized and the electrical potential distribution is solved using FEM. The results of the electrical potential along every trajectory is then exported as extracellular (Ext.) potential to the cable model of the fibres where they are used to generate a pulsed signal in a similar fashion as the intended stimulus. This method is valid under quasi-static approximation.

manual segmentation time during the construction of head model compartments. Before the segmentation process, a Recursive Gaussian filter was applied on the data sequence to reduce the background noise.

The skin, eyeball, muscle, skull and brain layers were segmented based on the image dataset using a combination of automatic and manual segmentation techniques as shown in Fig. 1. Each component of the tissue types were represented by a *mask* to modify the image as appropriate in ScanIP. Each mask was segmented based on an appropriate gray scale threshold range. It is worth noting that the mask sequence is important to prevent tissue layers overlapping during segmentation.

The SON and STN trajectories cannot be distinguished from the MRI images due to their relatively small diameters (i.e.,  $\sim 1\text{mm}$ ) [3] but they were obtained from the literature [11], [12]. 3D models of the nerves were manually constructed in ScanIP. Only the left branches of the nerves were considered in this paper due to the symmetry of the human head. A trajectory of STN and four variations of SON were constructed to investigate the current threshold for each nerve model. The statistically average nerve position was shifted along the forehead based on reported standard deviations in the literature [11]. These nerves were named as STN, SON1, SON2, SON3 and SON4, where SON4 is the one which is furthest away from the center of the forehead.

#### B. Finite Element Method

For all the subsequent simulations and operations a computer with an Intel Core i7-6700 CPU @ 3.4 GHz with 64 GB RAM was used.

Based on the segmented data, a 3D human head model was constructed in ScanIP as shown in Fig. 1. An external boundary (i.e., a sphere) was also constructed. The domains were discretized using tetrahedral elements. To ensure sufficient accuracy, the maximum element size was adjusted in the regions of interest. Whilst skin, muscle, electrode patch and nerves were finely meshed, brain, skull and air layers were relatively coarsely meshed. This resulted in approximately 1.4 million elements, corresponding to 4.5 hours of discretization time. Further tests indicated this to be a sufficiently high level of discretization.

The generated mesh was imported into COMSOL Multiphysics v5.2a (COMSOL, Ltd., Cambridge, U.K.). The current level was set to be 1 mA through the anode and -1 mA through the cathode while defining them as equipotential surfaces. This was an arbitrary unit level to be scaled at the subsequent stages. A Dirichlet boundary condition ( $V=0$ ) was set at the outer boundary of the model (i.e., the sphere). A quasi-static approximation of Maxwell's equations was used as shown in (1) and the differential equations were solved using finite element methods (FEM).

$$\nabla \cdot (\sigma \nabla V) = 0 \quad (1)$$

TABLE I. TISSUE LAYERS AND THEIR CONDUCTIVITY

Tissue layers	Conductivity(S/m)	Reference
Skin	0.43	[18]
Muscle	0.16	[19]
Nerve	1.2	[19]
Eyeball	0.5	[19]
Skull	0.015	[20]
Brain	0.1	[19]
Gel	0.1	-

where  $\sigma$  is the conductivity of each medium and  $V$  is the electrical potential in the corresponding geometry. The conductivity of the external boundary was set to 1e-10 S/m and that of each tissue was set as shown in Table I (as reported in the literature for low frequencies). Exact methods of implementing the quasi-static approximation in COMSOL may be found in [15].

The radius of the external sphere was changed from 0.25 m to 10 m gradually. Only a shift in the voltage along the nerve trajectory was observed. This variation was less than 2% when the radius was changed from 0.5 m to 1 m. Thus the radius of the external medium was set to 0.5 m.

### C.Frontal Nerve Axon Model

To detect nerve fiber excitation, a double layer cable model of myelinated fibers in the frontal nerve were developed with imperfect myelin insulation and implementing McIntyre-Richardson-Grill channel mechanisms for the nodes of Ranvier [13]. The compartments between two nodes comprised two myelin attachments, two paranodal and ten internodal compartments. This ensures a smooth electrical potential variation.

$\text{A}\beta$  fibers, whose diameters followed a Gaussian distribution with a mean of  $\mu_D = 12.5 \mu\text{m}$  and standard deviation of  $\sigma_D = 2 \mu\text{m}$ , were modeled based on experimental data [14] while the associated parameters were derived by interpolating experimental measurements [13] as shown in [15]. The first node of Ranvier was randomly placed between 0 and  $\Delta x$  of the arc-length of the related nerve, where  $\Delta x$  is node to node distance for a given fiber. The compartments were inserted between every two active nodes along the nerve trajectory and the fiber model was terminated by a node [15] based on the trajectory defined in the FEM model. This process was repeated for all 100 fibers in the nerve. The models were imported in NEURON v7.4 [16] to solve the underlying differential equations using the Backward Euler integration method with 25  $\mu\text{s}$  steps.

The electrical potential along the nerve was solved in COMSOL, interpolated in Matlab, and imported as extracellular potentials in NEURON as depicted in Fig. 1. In

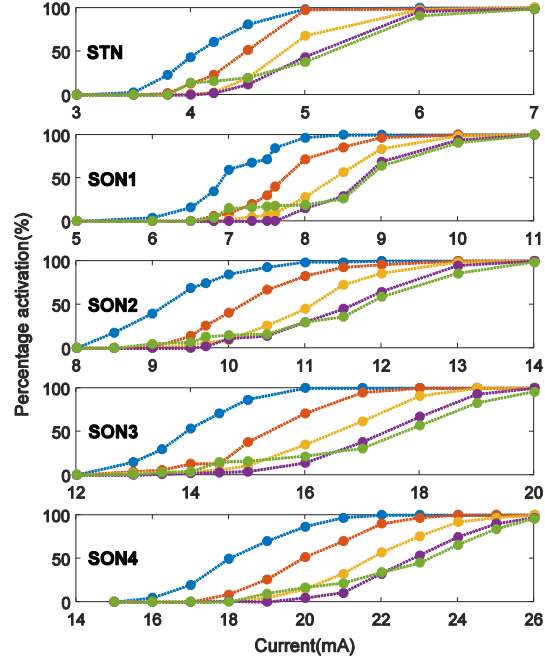


Figure 2. PA of fibers versus stimulus current amplitude for different pulses in STN and four variations of SON, where SON4 is the variation furthest away from the centre of the temple. These variations are within the limits reported in the literature. The stimulus was 250  $\mu\text{s}$  pulses repeated at 60 Hz. The first, second, third, fourth and fifth pulses are shown in blue, orange, yellow, pink and green, respectively.

NEURON, the extracellular potentials were pulsed as biphasic pulses of 250  $\mu\text{s}$  repeated at 60 Hz as used in [7]. For different amplitudes, the values were simply multiplied which is appropriate under quasi-static approximation. The percentage activation (PA) of the fibers was measured for 5 consecutive pulses. The number of pulses was dictated by the fact that only in the fifth pulse the level of current for PA = 50% was similar to the previous pulse (i.e. fourth pulse) as shown in Section III.

### III. RESULTS

The PAs of the fibers with respect to the required stimulus current levels for all different nerve variations and all the 5 consecutive pulses are shown in Fig. 2.

To assess the PA, only the fifth pulse is considered as described above. The fibers in the furthest nerve (SON4) from the electrodes require higher current thresholds to elicit the same PA, compared to the nerve fibers placed close to the center of the forehead. The STN is situated nearly under the anode electrode in the model, and nerve fibres are activated at a relatively lower current level when compared with the rest of the nerves. STN required 4 mA current to generate action potential and reached PA=100% at about 6 mA amplitude. The minimal stimulus current thresholds for fibers in the SON1, SON2 and SON3 were 7 mA, 9.5 mA and 14 mA, respectively. The fibers in the SON4 nerve required at least 19 mA to be minimally activated. To

achieve PA=100% for SON4, 26 mA stimulus current was required.

#### IV. DISCUSSION

Hybrid models can be used in the design and development of neural prosthetics and their optimization. In such models, the electrical potential field is calculated in a volume conductor model which is then exported to a cable model as extracellular potential to predict the response of the nerve [15], [17].

In this paper, the influence of the nerve variations on the nerve activation was investigated based on hybrid models. Since STN and SON branches of the frontal nerve may cause migraine, the STN and SON were the target of this study. Although these nerves have multiple finer branches, only the main trunks of the nerves were considered as they are likely to be the main cause of activation. It was shown that the variation of the position of the nerve has an impact on the stimulus current level required. It was also observed that the PA level remains constant after the fourth pulse at the corresponding excitation levels for the stimulus pulse parameters used here (biphasic 250  $\mu$ s pulses repeated at 60 Hz [7]). The range of currents required (6mA to 26 mA) is in agreement with published data in the literature [7]. Thus, the accuracy of the results is retrospectively verified.

The fact that the variations of the nerve position may introduce a 400% increase in the required current level to achieve the same level of PA shows the need for a more elaborate neuromodulator electrode setting design. This may also indicate why the efficacy of the existing design is low in some cases.

#### V. CONCLUSION

A realistic volume conductor model of a human head, TENS and a cable model of mammalian nerve fibre has been used to assess the effects of certain nerve variations on the required stimulus current. Although electrodes are relatively large to cover the central section of the forehead, the results indicate that when the nerve is shifted away from the center of the forehead, stimulus current threshold level may be increased for all nerve variations. This shows that the relatively mixed results due to the existing design may be attributed to the nerve variations as reported in the literature [11] and implemented in this paper.

Although these results are in agreement with the previously published patient data [7], more accurate results and detailed conclusions may be drawn by modeling the neuroanatomical structures in more detail. Furthermore, a more elaborate matrix of variation parameters, taking into account the variations of the nerve, head, various segmentation layers and nerve fibres may be developed to generate a realistic ensemble of variations to produce a statistically relevant patient group to more accurately assess the effect of variations. The results can in turn be used to design a more effective neuromodulator based on specific effects of the variations.

#### REFERENCES

- [1] T. J. Steiner, L. J. Stovner, and G. L. Birbeck, "Migraine: the seventh disabler," *J. Headache Pain*, vol. 14, p. 1, Jan. 2013.
- [2] T. J. Steiner, G. L. Birbeck, R. H. Jensen, Z. Katsarava, L. J. Stovner, and P. Martelletti, "Headache disorders are third cause of disability worldwide," *J. Headache Pain*, vol. 16, p. 58, Jan. 2015.
- [3] J. E. Janis et al., "Anatomy of the Supratrochlear Nerve," *Plast. Reconstr. Surg.*, vol. 131, no. 4, pp. 743–750, 2013.
- [4] P. J. Goadsby, "Recent advances in understanding migraine mechanisms, molecules and therapeutics," *Trends Mol. Med.*, vol. 13, no. 1, pp. 39–44, 2007.
- [5] A. M. Blumenfeld et al., "Patterns of use and reasons for discontinuation of prophylactic medications for episodic migraine and chronic migraine: results from the second international burden of migraine study (IBMS-II)," *Headache*, vol. 53, no. 4, pp. 644–55, Apr. 2013.
- [6] P. D. Wall and W. H. Sweet, "Temporary abolition of pain in man," *Science*, vol. 155, no. 3758, pp. 108–9, Jan. 1967.
- [7] F. Riederer, S. Penning, and J. Schoenen, "Transcutaneous Supraorbital Nerve Stimulation (t-SNS) with the Cefaly® Device for Migraine Prevention: A Review of the Available Data," *Pain Ther.*, pp. 135–147, 2015.
- [8] J. Schoenen et al., "Migraine prevention with a supraorbital transcutaneous stimulator: A randomized controlled trial," *Neurology*, vol. 80, no. 8, pp. 697–704, 2013.
- [9] D. Magis, S. Sava, T. S. d'Elia, R. Baschi, and J. Schoenen, "Safety and patients' satisfaction of transcutaneous supraorbital neurostimulation (tSNS) with the Cefaly® device in headache treatment: a survey of 2,313 headache sufferers in the general population," *J. Headache Pain*, vol. 14, p. 95, 2013.
- [10] M. I. Iacono et al., "MIDA: A Multimodal Imaging-Based Detailed Anatomical Model of the Human Head and Neck," *PLoS One*, vol. 10, no. 4, p. e0124126, Apr. 2015.
- [11] K. N. Christensen, N. Lachman, W. Pawlina, and C. L. Baum, "Cutaneous Depth of the Supraorbital Nerve," *Dermatologic Surg.*, vol. 40, no. 12, pp. 1342–1348, 2014.
- [12] A. K. D. Harold Ellis, Bari M Logan, *Human Sectional Anatomy*, Third Edit. London: Hodder Arnold, 2009.
- [13] C. C. M. C. Intyre, A. G. Richardson, W. M. Grill, C. Cameron, A. G. Richardson, and M. Warren, "Modeling the Excitability of Mammalian Nerve Fibers: Influence of Afterpotentials on the Recovery Cycle," pp. 995–1006, 2002.
- [14] C. D. Vargas and A. Sirigu, "The Know-How of Face Transplantation," pp. 207–212, 2011.
- [15] A. N. Shiraz, M. Criggs, B. Leaker, and A. Demosthenous, "Minimizing Stimulus Current in a Wearable Pudendal Nerve Stimulator Using Computational Models," *IEEE Trans. Neural Syst. Rehabil. Eng.*, vol. 24, no. 4, pp. 506–515, 2016.
- [16] M. L. Hines and N. T. Carnevale, "The NEURON Simulation Environment," *Neural Comput.*, vol. 9, no. 6, pp. 1179–1209, Aug. 1997.
- [17] S. Raspopovic and M. Capogrosso, "A computational model for the stimulation of rat sciatic nerve using a transverse intrafascicular multichannel electrode," *Ieee Trans.*, 2011.
- [18] R. N. Holdefer, R. Sadleir, and M. J. Russell, "Predicted current densities in the brain during transcranial electrical stimulation," *Clin. Neurophysiol.*, vol. 117, no. 6, pp. 1388–97, Jun. 2006.
- [19] C. Gabriel et al., "The dielectric properties of biological tissues: I. Literature survey," *Phys. Med. Biol.*, vol. 41, no. 11, pp. 2231–2249, Nov. 1996.
- [20] T. F. Oostendorp, J. Delbeke, and D. F. Stegeman, "The conductivity of the human skull: results of *in vivo* and *in vitro* measurements," *IEEE Trans. Biomed. Eng.*, vol. 47, no. 11, pp. 1487–92, Nov. 2000.